Kinetic analysis of the thermal release of pyrene from commercial Carbon Black nanoparticles using a distributed activation energy model

M. Ströbele*, T. Häber, H. Bockhorn

Karlsruhe Institute of Technology (KIT), Engler-Bunte-Institute, Division of Combustion Technology (EBI-VBT), Engler-Bunte-Ring 1, 76131 Karlsruhe, Germany

Abstract

This research investigates the concentration effect of the thermal release of adsorbed polyaromatic hydrocarbons (PAHs) from commercial carbon black nanoparticles (CBNP) by using thermogravimetric analysis (TGA). Pyrene was used for this study as a representative of PAHs and Printex 90 as representative of commercial CBNP. The thermal desorption occurs in two stages. A non-isothermal, 1st-order distributed activation energy model (DAEM) including a Weibull distribution was used for numerically fitting of the second desorption stage. A kinetic compensation effect was observed. The trend of the mean activation energy and the standard deviation in dependence on the pyrene content could be expressed independently of the pre-exponential factor by choosing a reference value.

Introduction

Worldwide carbon black nanoparticles (CBNPs) production is about 10 million tons per year. It is mainly used in rubber products, predominantly in tires and also as a pigment in printer inks, paints and plastics. CBNPs are produced by incomplete combustion of hydrocarbons. Polycyclic aromatic hydrocarbons (PAHs) occur in the flame and act as precursors to CBNPs. After synthesis CBNPs contain considerable amounts of PAHs. These adsorbed PAHs are not tightly bound on the surface and can desorb.

The International Agency for Research on Cancer (IARC) has evaluated twelve PAHs as proven, probable or possible carcinogens in humans [1] and the World Health Organization (WHO) has classified carbon black nanoparticles as a potential carcinogen for humans [2]. It is not clear to what extend the potential danger is emanating from the nanoparticles themselves or by the PAHs accumulated on the surface. Thus, an understanding of how binding to CBNP changes the availability of PAHs is important for evaluating the health consequences and effects of these compounds.

In the literature, there are only few publications about the desorption kinetics of PAHs under non-isothermal conditions. The desorption conditions of PAHs from soot under isothermal conditions was examined by Guilloteau et al. [3] [4] [5].

Ghosh et al. [6] and Talley et al. [7] investigated the non-isothermal desorption behavior of PAHs on sediments. The thermal desorption profiles observed in this work are similar to those in these papers. They tried to describe the kinetics with the following models: Peak temperature method, Chan-Aris-Weinberg method, leading edge method, nonlinear curve fitting and various diffusion-based models. None of the models could give an accurate description of the desorption profiles. Therefore, a first order distributed activation energy model (DAEM) was used for the determination of kinetic parameters in this work. It is assumed that pyrene is adsorbed in layers on the CBNPs and the desorption from each of the layers has a different activation energy. The desorption signal is then an overlap of the contributions from all of these layers.

The DAEM model was proposed by Pitt [8] and further developed by Anthony and Howard [9]. A complex reaction is described herein by a number of parallel first-order reactions. Each of them has its own activation energy and all of the reactions have the same pre-exponential factor. The difference in activation energies can be represented by a continuous distribution function, like the Weibull distribution. The DEAM with Weibull distribution is used often to model the non-isothermal pyrolysis of biomass [10] [11].

The present paper shows the desorption behavior of PAHs dependent on the concentration during non-isothermal measurements. In addition, the kinetics of the second desorption stage was described by a first order DAEM based on a Weibull distribution for the activation energy.

Materials and Methods

Sample preparation

For this study, pyrene for synthesis (Merck Schuchardt OHG, Hohenbrunn) was used as a representative of PAHs and Printex 90 (Evonik Carbon Black GmbH, Frankfurt) as a representative of commercial CBNP. Pyrene was dissolved in diethyl ether and Printex 90 was suspended in the solution to prepare the samples. Homogenization was achieved by ultrasonic bath treatment. Diethyl ether was removed from the sample by evaporation at room temperature overnight. The samples with a pyrene content above 10 % were prepared by an accurate weighing of the two components. To adjust the pyrene content for samples with PAH content below 10 %, a sample with a pyrene content of 15.7 % was subsequently isothermally heat-treated. The time of the isothermal heat treatment, the temperature and the remaining pyrene content are shown in Table 1.

* Corresponding author: Michael.Stroebele@kit.edu

Table 1: Isothermal treatment conditions of samples with pyrene content of 15.7 % and the remaining pyrene contents after thermal treatment.

isotherm temperature [° C]	time [h]	pyrene content after treatment [%]
250	24	2.0
200	24	3.7
150	20	5.9
150	10	6.4
125	36	7.6
100	99	8.5

TGA-Measurements

Non-isothermal thermogravimetric measurements have been performed with a TG 201 F1 Libra (Netzsch, Selb) thermogravimetric balance. The heating rate was 10° C / min in helium flow of 100 ml / min to reach a final temperature of 900° C. Approximately 30 mg of each sample was weighed in a ceramic sample holder for the measurements.

DEAM

The time or temperature-dependent change of the degree of conversion is commonly used in the solid-state kinetics of thermal analysis. The degree of conversion is defined as:

$$\alpha_i = \frac{m_{0,i} - m_{t,i}}{m_{0,i} - m_{\infty,i}} \tag{1}$$

Where $m_{0,i}$ is the mass of the i-th part at the initial value, $m_{\infty,i}$ its final value and $m_{t,i}$ its mass at time t. The formal kinetics of desorption can be described by the following first order approach:

$$\frac{d\alpha_i}{dt} = k(T)\left(1 - \alpha_i(t)\right) \tag{2}$$

Provided that no chemical reaction occurs with a reactant, a desorption process usually occurs as a first order reaction. Therefore, a first-order reaction is assumed [5]. The temperature dependence of the reaction rate constant can be described by the Arrhenius approach, where k_0 is the pre-exponential factor, E_i the activation energy in the i-th part and R is the ideal gas constant.

$$k(T) = k_0 \cdot \exp\left(-\frac{E_i}{RT}\right) \tag{3}$$

Together with the introduction of the heating rate β = dT / dt for non-isothermal measurements, this results in:

$$\frac{d\alpha_i}{dT} = \frac{k_0}{\beta} \cdot \exp\left(-\frac{E_i}{RT}\right)(1 - \alpha_i) \tag{4}$$

In a distributed activation energy model (DAEM) it is assumed that all reactions have the same pre-exponential factor and the reactions are intense enough to express the activation energy as a function f (E), where α·f(E)dE represents the share of the degree of conversion which has an activation energy between E and E+dE

$$d\alpha = \alpha \cdot f(E)dE \tag{5}$$

With this α_i in Equation (4) is replaced by α. Integration of Eq. 4 this leads to:

$$\alpha = \int_0^\infty \exp\left[-\int_{T_0}^T \frac{k_0}{\beta} \cdot \exp\left(-\frac{E_i}{RT}\right) dT\right] f(E)dE \tag{6}$$

The Weibull distribution is used for the activation energy distribution [12]. This distribution can be mapped with other distributions. For λ = 1, the Weibull distribution results in an exponential distribution. With a suitable choice of parameters, it could also depict a Gaussian or Rayleigh distribution. The Weibull distribution [13], [14] is given by:

$$f(E) = \frac{\lambda}{\eta} \cdot \left(\frac{E-\gamma}{\eta}\right)^{\lambda-1} \exp[\left(\frac{E-\gamma}{\eta}\right)^{\lambda}] \tag{7}$$

where λ is the shape parameter, η is the width parameter and γ is the activation energy threshold ($E \geq \gamma$). The mean activation energy E_0 and the standard deviation σ of the Weibull distribution are given by

$$E_0 = \gamma + \eta\Gamma\left(1 + \frac{1}{\gamma}\right) \tag{8}$$

$$\sigma = \sqrt{\eta^2\Gamma^2\left(\frac{2}{\lambda} + 1\right) - \eta^2\Gamma^2\left(\frac{1}{\lambda} + 1\right)} \tag{9}$$

where Γ is the Gamma function.

Equation 6 and Equation 7 lead to the final form for the DEAM including the Weibull distribution:

$$\alpha = \int_\gamma^\infty \exp\left[-\int_{T_0}^T \frac{k_0}{\beta} \cdot \exp\left(-\frac{E_i}{RT}\right) dT\right] \frac{\lambda}{\eta} \cdot \left(\frac{E-\gamma}{\eta}\right)^{\lambda-1} \exp[\left(\frac{E-\gamma}{\eta}\right)^{\lambda}] dE \tag{10}$$

The equation contains a double integral. In order to save computing time, the temperature integral was replaced by an approximation. In this work, the approach of Cai et al. [11] was used.

$$\int_{T_0}^T \exp\left(-\frac{E}{RT}\right) dT = \frac{E}{R}[p(u) - p(u_0)] \tag{11}$$

with

$$u = \frac{E}{RT}, u_0 = \frac{E}{RT_0} \tag{12}$$

and

$$p(u) = \frac{e^{-u}}{u^2} \frac{u + 0.25403\ln(u) + 0.36665}{u + 2.4598\ln(u) + 0.241457} \tag{13}$$

A Mathematica program was developed to solve the equation numerically. The Gauss Kornrod Rule was used for the integration. The frequency factor and the three

Weibull parameters were fitted to the measured data. Thereafter, the mean activation energy E_0 and its standard deviation σ were calculated.

Results and Discussion

TG-measurements

The thermal desorption of pyrene from samples with pyrene contents above 10 % shows two desorption stages. The thermogravimetric curves (TG) and their derivatives (DTG) are given in Figure 1.

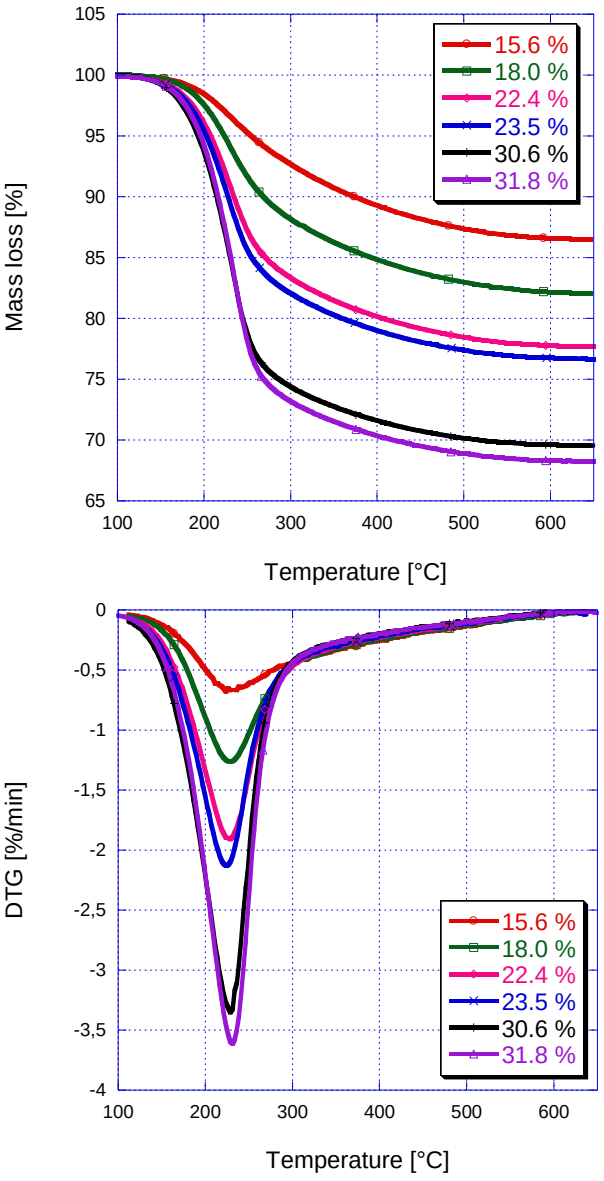

Figure 1: TG (top) - and DTG (bottom) - curves of pyrene from Printex 90 with two desorption stages.

The first desorption stage appears in a temperature range of about 100 to 300° C. The desorption rate increases with increasing pyrene content. The peak of DTG curves corresponds to the maximum rate of desorption. Its position at about 230° C is independent of the pyrene content. The maximum of the DTG curves remain at constant temperatures for a 1st-order desorption, whereas it shifts with increasing initial cover to higher temperatures for zero-order desorption and to lower temperatures for higher-order desorption. Therefore, it can be concluded that the first desorption stage is a 1st-order desorption. The subsequent second desorption stage is flatter and extends over a wider temperature interval up to 650° C. The desorption rate is much slower than in the first desorption stage.

Figure 2 shows the TG and DTG curves of two samples having different initial weights but the same pyrene content of about 27 %. Because the samples are prepared in ceramic crucibles of the same diameter, different initial weights correspond to different sample heights in the crucible. The first desorption stage shifts to higher temperatures with increasing sample weight, whereas the second desorption stage remains unchanged. This is probably due to transport processes through the sample layers in the crucible.

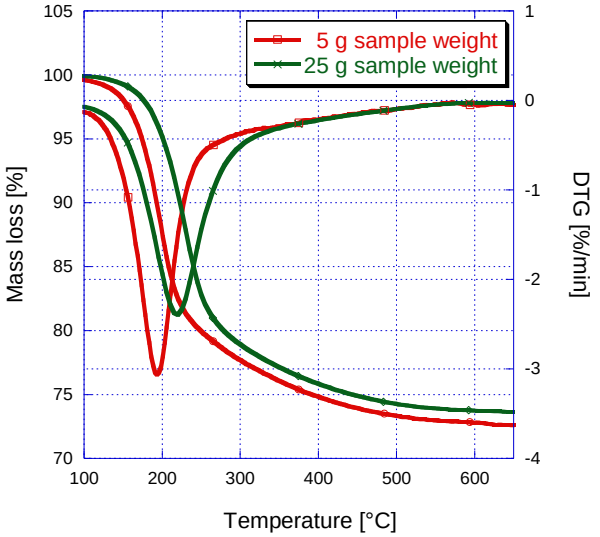

Figure 2: TG - and *DTG - curves of pyrene from Printex 90 with different sample weights.*

For investigating the second desorption stage measurements were carried out with pyrene contents below 10 %. The TG curves and DTG curves of the CBNP samples with different contents of pyrene below 10 % are shown in Figure 3. With increasing pyrene content the thermal release starts at lower temperatures. The DTG peak shifts with increasing pyrene content to lower temperatures, however, the desorption rate after the DTG peak is the same for all samples. In the temperature range before the DTG peak, the desorption rate increases with pyrene content. A complete release is always attained at about 650° C. The desorption starts at temperatures of approximately 120° C for the sample with a pyrene content of 8.5 %. This temperature is below the final temperature of the first desorption stage of the samples with a pyrene content of more than 15.6 %, see Figure 1. This suggests that the two desorption stages overlap.

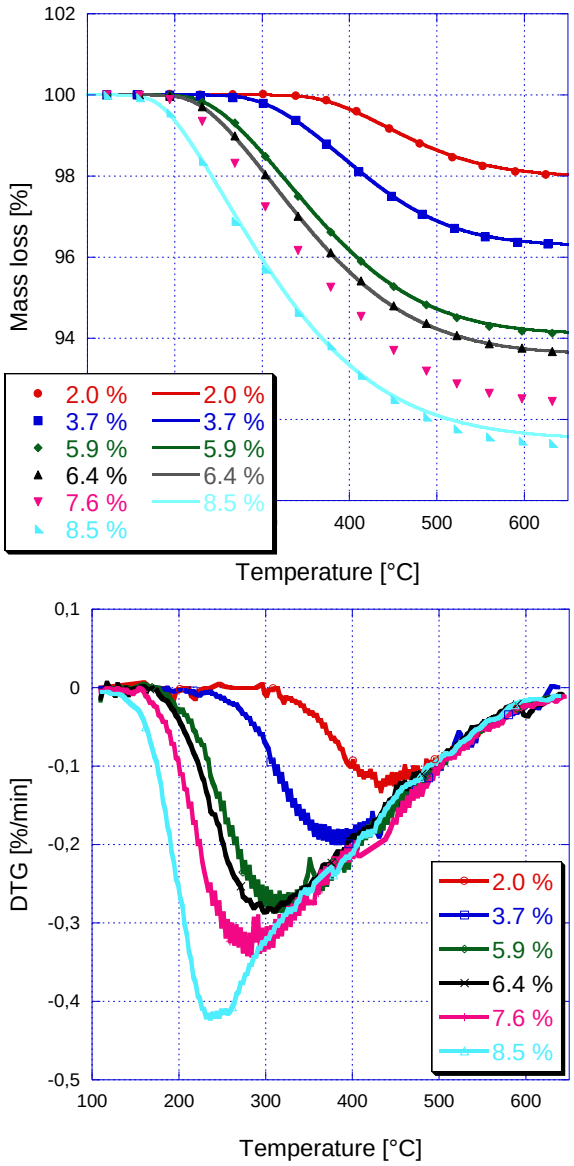

Figure 3: TG- (top) and DTG- (bottom) curves of pyrene from Printex 90 with different contents of pyrene and the comparison of the TG-curves between the measured data (dots) and the fitted curves (lines).

Kinetic modeling

Printex 90 consists of approximately spherical primary particles, which form aggregates and agglomerates. It is assumed that pyrene initially accumulates in the gaps between the particles and once they are filled, accumulates in layers on the aggregates or agglomerates. Pyrene from these layers on the aggregates or agglomerates desorb in the first stage. The rate is proportional to the number of molecules remaining on the surface and the molecules are independent of each other. All Pyrene molecules have the same activation energy independent of their positions. The activation energy of the pyrene molecules, which are in the gaps between the primary particles, depends on the location. The bonds become weaker with an increasing distance from the particles, while the bonding strength of the subjacent layers does not change. Therefore, the DEAM model is used for modelling the kinetics.

In Table 2, the pyrene content, the logarithm of pre-exponential factor log (k_0), the mean activation energy E_0 and its standard deviation σ for the samples with pyrene contents below 10 % are given. As is obvious from the data, there is no clear correlation between E_0 and log (k_0). Therefore, log (k_0) was predefined and fixed in further calculation of E_0, starting with the values given in Table 2.

Table 2: The pyrene content, logarithm of pre-exponential factor log (k_0), mean activation energy E_0 and standard deviation σ for the desorption of pyrene from Printex 90 samples with a pyrene content below 10%.

pyrene content [%]	log (k_0) [-]	E_0 [kJ / mol]	σ [kJ / mol]
2.0	13.6	226 648	22 283
3.7	17.2	256 451	30 129
5.9	17.1	239 238	35 378
6.4	18.8	252 808	38 338
7.6	15.7	215 133	35 651
8.5	14.3	189 521	33 672

The mean activation energy obtained in this way is plotted against different values of log (k_0) in Figure 4. From the Figure a kinetic compensation effect is obvious. This effect describes a linear relationship between the frequency factor and activation energy [15]. It is given by log (k_0) = m E_0 + c, where m and c are variables. All pairs of values of log (k_0) and E_0 respectively σ, which can be described by this linear equation, represent mathematically correct results of the DEAM. Absolute values can be only obtained, if the correct pre-exponential factor is known.

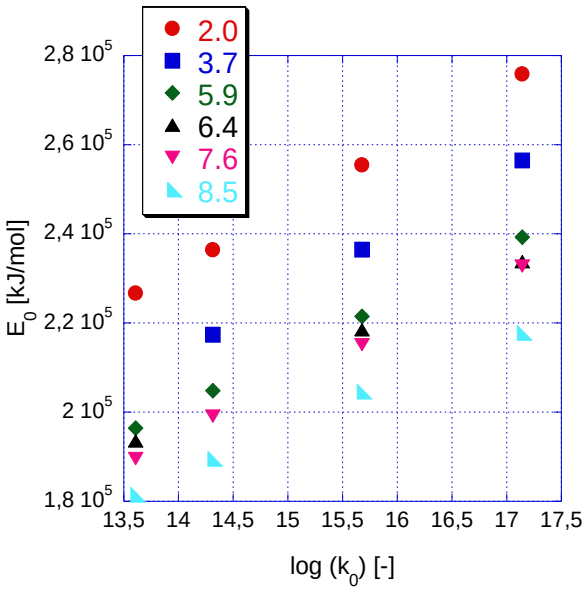

Figure 4: E_0 plotted against log (k_0) for the samples with a pyrene content below 10 %.

In Table 3 the pyrene content, the logarithm of pre-exponential factor log (k_0) with a value of 13.6, the mean activation energy E_0 and the standard deviation σ are shown.

Table 3: The pyrene content, the pre-exponential factor log (k_0), mean activation energy E_0 and standard deviation σ of Printex 90 samples fitted with a constant log (k_0).

pyrene content [%]	log (k_0) [-]	E_0 [kJ / mol]	σ [kJ / mol]
2.0	13.6	226 648	22 283
3.7	13.6	210 076	24 547
5.9	13.6	196 427	29 012
6.4	13.6	193 544	29 979
7.6	13.6	189 613	31 034
8.5	13.6	181 450	32 426

It can be seen that the mean activation energy decreases with increasing content and the standard deviation increases. Figure 3 shows the good agreement between the measured data (dots) and the fitted data (lines) for a constant log (k_0) of 13.6. This good correlation and the increase of E_0 and the decline of σ, with increasing pyrene content, support the assumption of the above sketched theory.

In order to elucidate the change of E_0 respectively σ in dependence on the pyrene content and the independancy of log (k_0), E_0 and σ, respectively, the results with a pyrene content of 2.0 % was taken as a reference point. The ratios of E_0 with a constant log (k_0) were calculated with the formula $E_{0,x} / E_{0,2.0}$, where $E_{0,x}$ is E_0 at pyrene content of x % and $E_{0,2.0}$ is E_0 at a pyrene content of 2.0 %. The ratios of σ were calculated the same way. Table 4 shows the results of the calculations with constant log (k_0) of 13.6, 14.3, 15.7 and 17.1. The Table can be read as follows: The E_0 of a sample with a pyrene content of 5.9 % is 87 % of the E_0 of a sample with a pyrene content of 2.0 %. It is noticeable that the deviation of the calculations with different constant log (k_0) for the standard deviation is higher than for the mean activation energy.

Table 4: The ratios of $E_{0,x}$ to $E_{0,2.0}$ and of σ_x to $\sigma_{2.0}$ against the pyrene content. The deviations refer to the results of the calculations with log (k_0)s of 13.6, 14.3, 15.7 respectively 17.1.

pyrene content [%]	$E_{0,x} / E_{0,2.0}$ [-]	$\sigma_x / \sigma_{2.0}$ [-]
2.0	1.00	1.00
5.9	0.87 ± 0.00	1.29 ± 0.01
6.4	0.85 ± 0.00	1.36 ± 0.02
7.6	0.84 ± 0.00	1.42 ± 0.02
8.5	0.80 ± 0.01	1.44 ± 0.02

Figure 5 shows the ratios in dependency of the pyrene content for log (k_0) of 13.6, 14.3, 15.7 and 17.1. A linear trend line was fitted to the data. The equation for the mean activation energy is $E_{0,x} / E_{0,2.0} = -0.0310 \cdot x + 1.0589$ and for the standard deviation $\sigma_x / \sigma_{2.0} = 0.0705 \cdot x + 0.8641$. With this linear equation, it should be possible to predict values for E_0 and σ for unknown pyrene contents in that range.

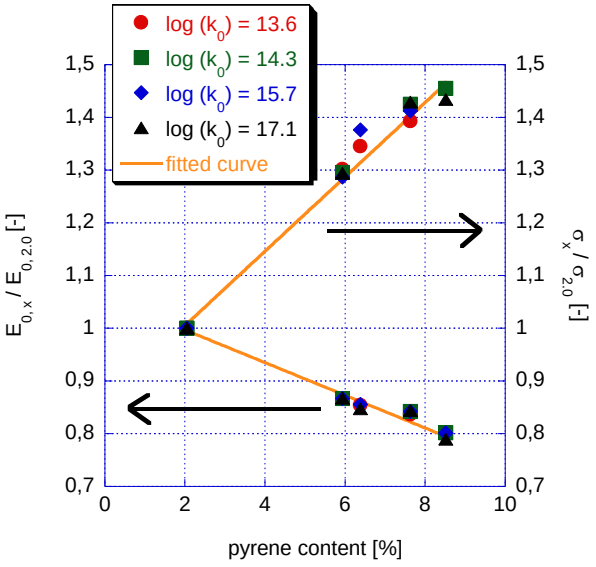

Figure 5: The ratios of $E_{0,x}$ to $E_{0,2.0}$ and of σ_x to $\sigma_{2.0}$ with log(k_0) fixed at 13.6, 14.3, 15.7 respectively 17.1 against the pyrene content.

Conclusion

The desorption of pyrene from Printex 90 shows two desorption stages. The first stage occurs at high content of pyrene and resembles a first order desorption. Depending on initial weight of the sample in the crucible, the temperature interval of the release moves. The second desorption stage shifts with decreasing pyrene content to higher temperatures. A non-isothermal, 1st-order distributed activation energy model (DAEM), based on a Weibull distribution of the activation energies was used to describe the second desorption stage. The agreement between the measured data and the calculated data is good. The frequency factor and the three Weibull parameters were fitted to the measured data. The expected value and the variance of the activation energy were calculated from the three Weibull parameters. By fixing the frequency factor the kinetic compensation effect can be excluded and the expected value and the variance of then activation energy from different runs can be compared. The trend of the mean activation energy and the standard deviation in dependence on pyrene content could be expressed independently of the pre-exponential factor by choosing a reference value. This is consistent with a desorption model where pyrene desorbs from different locations of the CB aggregates (surface, gaps etc.) with different activation energy.

Acknowledgements

This work was supported by the German Federal Ministry of Education and Research (BMBF) - program: "nanoCOLT - Long-term effect of modified carbon black nanoparticles on healthy and damaged lungs".

References

[1] IARC Working Group on the Evaluation of Carcinogenic Risks to Humans, IARC monographs on the evaluation of carcinogenic risks to humans, volume 92, some non-heterocyclic polycyclic aromatic hydrocarbons and some related exposures: This publication represents the views and expert opinions of an IARC Working Group on the Evaluation of Carcinogenic Risks to Humans, which met in Lyon, 11 - 18 October 2005, WHO, Lyon, 2010.

[2] N. Janssen, Health effects of black carbon, World Health Organization Regional Office for Europe, Copenhagen, 2012.

[3] Y. Bedjanian, M.L. Nguyen, A. Guilloteau, J. Phys. Chem. A 114 (2010) 3533–3539.

[4] A. Guilloteau, Y. Bedjanian, M.L. Nguyen, A. Tomas, J. Phys. Chem. A 114 (2010) 942–948.

[5] A. Guilloteau, M.L. Nguyen, Y. Bedjanian, G. Le Bras, J. Phys. Chem. A 112 (2008) 10552–10559.

[6] U. Ghosh, J.W. Talley, R.G. Luthy, Environmental science & technology 35 (2001) 3468–3475.

[7] J.W. Talley, U. Ghosh, J.S. Furey, S.G. Tucker, R.G. Luthy, Environmental Engineering Science 21 (2004) 647–660.

[8] Pitt G.J., Fuel (1962) 267–274.

[9] D.B. Anthony, J.B. Howard, AIChE J. 22 (1976) 625–656.

[10] J. Cai, W. Wu, R. Liu, Renewable and Sustainable Energy Reviews 36 (2014) 236–246.

[11] J. Cai, R. Liu, Bioresource Technology 99 (2008) 2795–2799.

[12] W.Q. Meeker, L.A. Escobar, Statistical methods for reliability data, Wiley, New York, ©1998.

[13] C.C. Lakshmanan, N. White, Energy Fuels 8 (1994) 1158–1167.

[14] J. Cai, R. Liu, J. Phys. Chem. B 111 (2007) 10681–10686.

[15] A.J. Fletcher, K.M. Thomas, Langmuir 16 (2000) 6253–6266.